Magnetohydrodynamic electrolyte flow within an inter-electrode gap driven by a sinusoidal electric field and constant magnetic field

C. Bradley[1], J. Samuel[2]
1. U.S. Army RDECOM-ARDEC, Benét Laboratories, Watervliet, NY 12189, USA
2. Department of Mechanical Aerospace and Nuclear Engineering, Rensselaer Polytechnic Institute, Troy, NY 12180, USA

Abstract: Pulsed electrochemical machining is a necessary extension to traditional ECM for small geometries and some high-performance materials like super alloys. Electrical current density is one of the limiting factors. The electrolyte flow in the inter-electrode gap can be assisted using a magnetic field to allow higher currents, but this creates a complex magnetohydrodynamic flow. This paper presents an experimental and computational study of electrolyte flow velocity in an IEG with a sinusoidal electric field within a constant magnetic field. The electrochemical impedance spectroscopy experiments used a 7075 aluminum anode in an $NaNO_3$ electrolyte that showed the effects of magnetic field intensity and input voltage frequency on the current within the electrochemical cell. Computational analysis of the electrochemical cell showed the relation between the electromagnetic inputs and flow velocity. By incorporating the experimental results into another computational analysis, the final simulation shows potential optimal operating conditions for magnetically assisted pulsed ECM.

Keywords: Magnetohydrodynamic (MHD) Electrochemical Impedance spectroscopy (EIS), Pulsed Electrochemical Machining (PECM)

1. Introduction

Manufacture of complex micro-scale parts such as biomedical devices and chemical reactors with an excellent surface finish from a wide range of high performance metals has required non-conventional manufacturing processes, such as electrochemical machining (ECM) and electrochemical finishing/polishing. ECM uses anodic dissolution of a workpiece anode in an electrolyte based on the shape and proximity of a tool cathode [1]. This process can be assisted using pulsed current between the electrodes, (PECM) [2] and additional reverse polarity pulses can further assist the electrochemical performance of the process by increasing accuracy [3]. Bipolar pulsed electric fields are used in an anodic dissolution electrochemical cell to remove the passivation layer from metals to increase surface quality and efficiency [3-6].

Since PECM relies on an electrolyte to transfer machining energy to the workpiece, there are electrochemical and fluid interactions that play a significant role in process performance [7]. From an electrochemical perspective, the literature on ECM discusses pulsed electric field effects on the electrical double layer (EDL) pseudo-capacitance that cause improvements in conductivity and, as a result. an increase in machining performance in terms of material removal rate (MRR) and surface finish [8, 9]. Externally applied magnetic fields are a common way to assist ECM performance [7, 10]. The Lorentz force acting on the electrolyte in the inter-electrode gap (IEG) increases with higher magnetic fields improving electrolyte flow and conductivity, which enhances ECM performance in terms of accuracy and surface finish [11-13]. Both PECM and magnetic fields can be combined for a dual-assisted anodic dissolution process that combines two different assistances to increase performance further [14-16]. This type of dual-assisted ECM will generate a complex magnetohydrodynamic (MHD) electrolyte flow in the IEG that will affect performance.

To better control the coupled effects of PECM in a magnetic field and improve ECM performance, the combined effects must be studied. Studies in the literature have considered the empirical performance effects of single assisted [2, 12, 13] or dual-assisted ECM involving PECM and magnetic fields [14-16], which does not address the specifics of leveraging the MHD aspects. Simulations of the MHD effects of ECM electrolyte within either a magnetic field [11, 17] or in a PECM cell [18] have given insight into a similar but fundamentally different system than the dual-assisted case.

Considering the above state-of-the-literature, this paper introduces a combination of electrochemical impedance spectroscopy (EIS) testing with an MHD simulation to represent a magnetically assisted anodic dissolution electrochemical cell. EIS testing gives insight into the effects of the EDL structure on the electrical impedance of the electrochemical cell. The EIS results then drive the current in the MHD

simulation to give a better understanding of the electrolyte flow within the IEG.

The EIS experimental results show that both the cell voltage frequency and magnet flux density are significant factors in cell electrical performance. The MHD simulation without the EIS data shows a significant but very different relation of voltage frequency and magnetic field to electrolyte flow velocity. When the computational analysis is combined with the EIS, the results suggest operating parameters that differ from either of the two individual results. While these findings indicate an operating regime of higher electrolyte velocities, whether that translates into increased machining performance, will require PECM validation experiments.

The remainder of the paper is structured as follows. Section 2 outlines the theory related to magnetically assisted PECM. Section 3 presents the details regarding the design of the experimental testbed. Section 4 discusses the computational analysis methodology and Section 5 discusses the findings. Finally, Section 6 outlines the specific conclusions that can be drawn from this study.

2. Theory

EIS is used to determine the impedance, in Ohms, of an electrochemical cell at different sinusoidal frequencies under given conditions - in this case a range of magnetic field intensities. The response of the cell to a sinusoidal input should give insights relevant to PECM frequency. An EIS scan measures the complex valued impedance as a function of input voltage and output current according to Ohm's law. Using the reciprocal of impedance, conductance (|**Y**|), Ohm's law is then,

$$I = |Y| \cdot V, \tag{1}$$

where I is the total primary current, V is the applied voltage. The magnitude of this conductance, $|Y|$, is then used to drive the applied sinusoidal primary current in the MHD simulation, which determines the current density, $\mathbf{J}_{cond}$.

The MHD simulation requires a solution for the electric and magnetic fields along with the incompressible laminar Navier-Stokes equations. The solution is separated into the time-dependent electric field solution without solving for the induced magnetic field. The low current densities considered in this paper are typical for a comparable PECM cell, and in practice the low current produces a magnetic field much smaller than the minimum field used in this research, making the approximation reasonable. The magnetic field is assumed constant in both time and space. The Lorentz force is then a function of current, velocity, and the magnetic field. That volume force is then added to the Navier-Stokes equations to solve for electrolyte velocity.

First the electric field must be solved in order to find the current density generated by the external potential applied across the electrochemical cell. Charge conservation is enforced using the equation for charge continuity in Eq. 2 and is a corollary to the Maxwell equations,

$$\nabla \cdot \mathbf{J}_{cond} = -\frac{\partial \rho_q}{\partial t}, \tag{2}$$

where $\mathbf{J}_{cond}$ is the current density and ρ_q is the charge density. The Maxwell-Faraday equation yields the general electric potential field **E**,

$$\mathbf{E} = -\nabla V - \frac{\partial \mathbf{A}}{\partial t}, \tag{3}$$

where V is the scalar electric potential, **A** is the magnetic vector potential. In order to simplify the problem, the changing magnetic field is not considered, yielding,

$$\mathbf{E} = -\nabla V. \tag{4}$$

The externally driven current density $\mathbf{J}_{cond}$ is then,

$$\mathbf{J}_{cond} = \sigma \mathbf{E} + \frac{\partial \mathbf{D}}{\partial t}, \tag{5}$$

where σ is the electrolyte volume conductivity and **D** is the electric displacement field.

The continuous form of the Lorentz force is [19],

$$\mathbf{F} = \rho_q \mathbf{E} + \mathbf{J} \times \mathbf{B}, \tag{6}$$

where $\boldsymbol{\rho}_q$ is charge density, **J** is the total current density, and **B** is the constant magnetic field. Solute salt ions will have a hydration shell surrounding them for a net neutral charge resulting in a zero-charge density, $\boldsymbol{\rho}_q$ in Eq. 6 [20]. This leaves only the cross product of current density with the magnetic field,

$$\mathbf{F} = \mathbf{J} \times \mathbf{B}. \tag{7}$$

The current density, J, in the electrolyte results from both electrode conduction in Eq. 5 and the induced current, $\mathbf{J}_{ind}$, from the electrolyte velocity, **u**, and the constant magnetic field, **B**, according to the Lorentz force in Eq. 8,

$$\mathbf{J}_{ind} = \sigma \mathbf{u} \times \mathbf{B}. \tag{8}$$

The total current density is then,

$$\mathbf{J} = \mathbf{J}_{cond} + \mathbf{J}_{ind.} \quad (9)$$

The constant magnetic field in Eq. 6 and Eq. 8 is a simplification mentioned earlier that ignores the induced magnetic field generated by the current density, **J**. With a solution for the Lorentz force per unit volume, **F**, this force can be applied as an external force in the Navier-Stokes equations.

The second step in solving this MHD problem is to determine the electrolyte velocity using the Navier- Stokes equations for laminar incompressible flow,

$$\rho\frac{\partial \mathbf{u}}{\partial t} + \rho(\mathbf{u}\cdot\nabla)\mathbf{u} = \nabla\cdot\left[-p\mathbf{I} + \mu\left(\nabla\mathbf{u} + (\nabla\mathbf{u})^{\mathrm{T}}\right)\right] + \mathbf{F} \quad (10)$$

where ρ is the fluid density, μ is the dynamic viscosity, p is the pressure, and **I** is the identity matrix. Equation 10 and Eq. 8 are coupled in **u** requiring a simultaneous solution. Since the flow is incompressible, the flow continuity equation simplifies to,

$$\rho\nabla\cdot(\mathbf{u}) = 0. \quad (11)$$

Now the solution for the electrolyte velocity, **u**, and pressure can be evaluated under various conditions. The EIS and simulation results each give insight into flow cell function. Using the EIS result to drive the simulation extends the results beyond either individual solutions.

3. Experimental design

This experimental study used a flat 7075 aluminum alloy workpiece (anode) and a 316 stainless steel tool (cathode). Table 1 lists the aluminum alloy composition, which is widely used in the aerospace industry [21]. The non-ferromagnetic 7075 aluminum and austenitic stainless steel were specifically chosen to leave the constant magnetic field unwarped by ferromagnetic effects [22]. The minimum magnetic field range was the locally estimated, earth magnetic field shown in Table 1. The present study focuses on MHD induced flow in an environment representative of PECM. The IEG was maintained at 390 μm in an electrolyte of 20% concentration $NaNO_3$, with no forced flow and a temperature of 21° ± 1° C. Sodium nitrate avoids the Cl^- ion corrosion of aluminum associated with NaCl [23]. Both tool and workpiece surfaces were polished down to a 3,000-grit abrasive. Table 1 summarizes experimental conditions for EIS testing. A cut-away of the 3D printed flow cell used to conduct the EIS testing in shown in Fig. 1. The permanent magnets shown are one of three sizes used in conjunction with their position to generate various magnetic field flux densities used in the experiments.

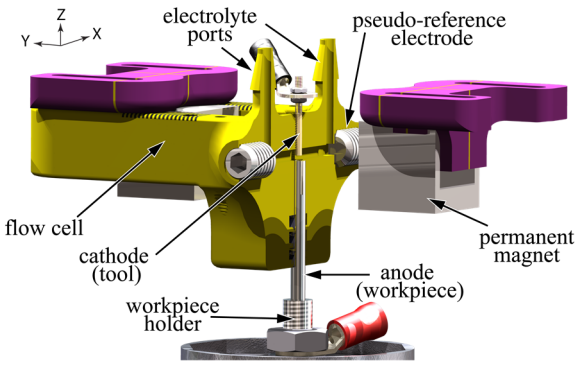

Figure 1. Model of experimental flow Cell

Table 1. Summary of experimental conditions

Workpiece	7075 aluminum alloy workpiece Al 89.3%, Cu 1.6%, Mg 25%, Other 1.0%, Zn 5.6%
Tool	1.5 mm diameter 316 stainless steel rod, insulated with acetal resin annulus
Process	-$NaNO_3$ Mass Concentration: 20% -Temperature: 20-22C -Inter-electrode gap: 390 μm
Electrical Input - **V**	- Voltage: ±0.10V - Frequency: 0.25 Hz - 250 kHz - Offset Voltage: 1.10V - 1.20V
Magnetic Field - **B**	- Flux Density: 0.053 mT - 935 mT
Output - |**Y**|	- Conductance: (mS)

A magnetic field map was created using an XY scanning table and an F.W. Bell 5080 gauss meter with a transverse probe. The field map for the 935 mT field is shown in Fig. 2 with the value on the Z-axis derived from the average of measurements within the tool area depicted with the inner cylinder. The outer cylinder depicts the workpiece. Only the magnetic field in the direction from one magnet face to the other was measured as the other directions were orders of magnitude smaller within the IEG.

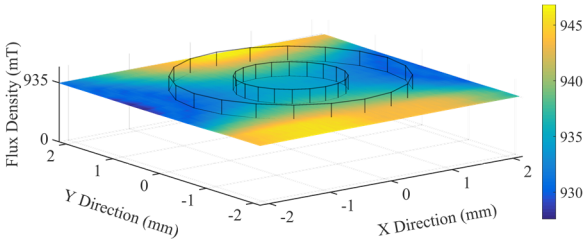

Figure 2. Map of magnetic field flux density within the IEG showing a small diameter for the tool and a larger diameter for the workpiece

EIS measurements were taken with a Princeton Applied Research, VeraSTAT3 electrochemical system that measured the impedance one frequency at a time. The spectrum was scanned on a logarithmic scale. Voltages are referenced to a pseudo-reference electrode of 316 stainless steel in contact with the electrolyte, where the open circuit potential is 0.8V [24]. The conductivity in an electrochemical cell is also a function of voltage as it determines whether the cell is operating in the mass transport limited or transpassive state of the EDL [25, 26]. ECM is typically conducted in the transpassive state so the sinusoidal voltage for the EIS scans was on top of a DC voltage to ensure measurements were in the transpassive state.

4. Numerical model

The simulation emulates the basic geometry used for the EIS experiments with the same tool and workpiece diameter, along with the same IEG and flow channel dimensions. Additionally, the electrolyte properties of conductivity (σ) and density (ρ) were matched. The computational analysis was conducted in COMSOL 5.2™ using the AC/DC module to solve Maxwell's equations and the Multiphisics™ module to solve the laminar Navier-Stokes equations.

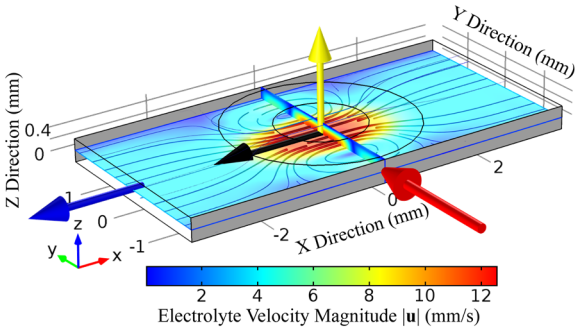

Figure 3. Simulation results showing vectors for magnetic field, electric field, Lorentz force, and resulting electrolyte flow with arrow, |**u**| surface, and stream lines

The diagram in Fig. 3 shows the geometry for the simulation with the instantaneous vectors representing the magnetic field shown in "red," the general electric field shown in "yellow," the general resulting Lorentz force in "black," and the general electrolyte flow shown in "blue."

The outer diameter shown in Fig. 3 represents the workpiece and defines the bounds of the IEG. The average velocity magnitude of the electrolyte within the IEG is used as the permanence metric for each time step. The maximum of this velocity is taken over the three frequency periods that each simulation runs and this velocity is the scalar performance metric used to compare simulations at each frequency and magnetic field. The sinusoidal current input for the MHD simulation has a constant amplitude, while the combined MHD simulation current is the product of a constant voltage and the corresponding conductivity ($|Y|$).

5. Results and discussion

The solution for the EIS testing indicates the relationship of the electrolyte conductivity, $|Y|$, as a function of magnetic flux density and the applied voltage frequency, which is of interest on its own as an indicator of electrochemical response. Likewise, the MHD solution, based on a constant amplitude sine wave, gives a more general indication of the flow effects in a given environment without regard to a specific electrochemistry. By combining the two solutions the result better represents the specific environment allowing a more directed study of magnetically assisted PECM.

5.1 EIS conductivity

In Fig. 4, the logarithmic surface that represents the conductivity, $|Y|$ is on a logarithmic scale in both the frequency and magnetic field axes. The conductivity surface was produced by averaging two tests each at three offset voltages ranging from 1.10V to 1.20V for a total of six for a given frequency and magnetic flux density.

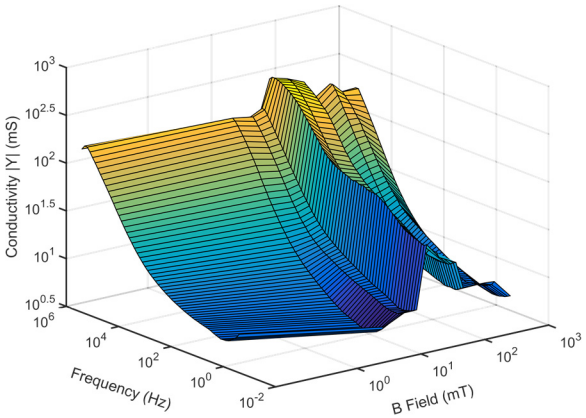

Figure 4. EIS conductivity as a function of frequency and magnetic field flux density

This result shows that higher frequency is directly proportional to conductivity, which is consistent with other studies [25, 27]. The relation between

conductivity and the magnetic field looks to have a maximum in the middle of the range around 46 mT, also similar in shape to another study [10].

5.2 MHD simulation

The simulation results shown in Fig. 3 was solved in the time domain over three sinusoidal periods at the same frequency and magnetic field at the matching EIS inputs. Figure 5 shows all the data used for the 935 mT simulation at a constant amplitude sinusoidal voltage input.

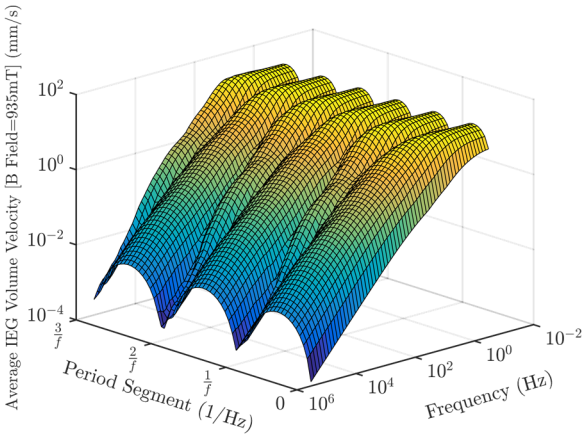

Figure 5. Electrolyte velocity magnitude averaged over the volume within the IEG at regularly spaced increments of waveform period for a 935 mT magnetic field

The simulation in Fig. 5 runs for three periods and the velocity magnitude at high frequencies shows three local maximums. During high frequencies, the electrolyte is accelerated during the positive portion of the sinusoid and is then decelerated during the negative portion for a directional pulsing effect. As the voltage *decreases* in frequency, the electrolyte flow begins to reverse direction more over time until the forward and reverse velocity magnitudes are equal from about 10 Hz and below. This is the velocity plateau in Fig. 5.

The maximum in the period direction of the surface in Fig. 5 forms the highest line representing the performance for a B field of 935 mT. Combining frequency performance across all the magnetic fields forms the surface plot in Fig. 6.

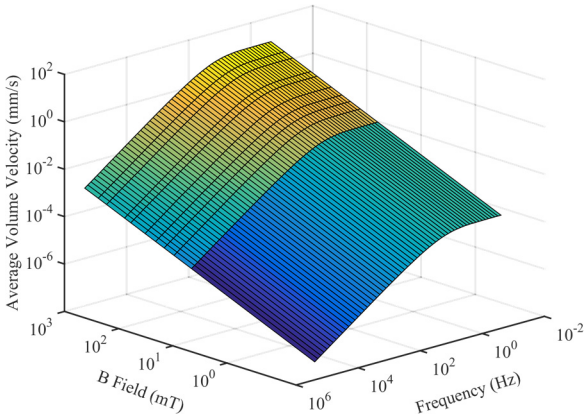

Figure 6. Electrolyte flow velocity as a function of electric field frequency and magnetic field flux density

The surface in Fig. 6 suggests operating at the highest magnetic field and at any frequency below roughly 10 Hz to maximize electrolyte velocity.

5.3 EIS driven MHD simulation

Since data was collected at the same levels in both the EIS and MHD simulations, combining the two required re-running the computational analysis. The surface plot for the combined simulation in Fig. 7 is similar to Fig. 6. The most prominent difference is that there is an apparent maximum for each magnetic field intensity around 10 Hz. The absolute maximum for velocity is still at the maximum magnetic field of 935 mT.

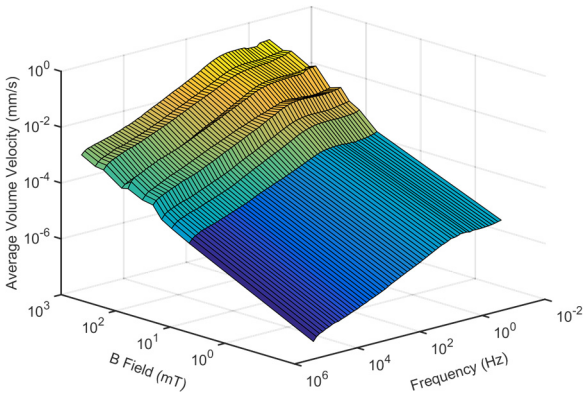

Figure 7. Electrolyte flow velocity as a function of electric field frequency and magnetic field flux density, where current flow is scaled according to the EIS determined conductivity

Conclusion

Both EIS testing and MHD simulations show that the electrolyte flow velocity within the IEG is highly dependent on both the electric field frequency and magnetic field flux density. The EIS results suggests

operating at a higher electric field frequency to maximize cell conductivity. The purely MHD computational result suggests minimizing the electric field frequency and maximizing the magnetic field to maximize electrolyte velocity. Combining the EIS results with the MHD computational analysis suggests an optimum electric field frequency to maximize the electrolyte flow velocity.

The results of this computational analysis will allow a more focused experimental validation of the effects of electric field frequency and magnetic field flux density on actual PECM machining performance. Using machining metrics like MRR, surface finish, and accuracy will give insight into where in the operating space the input parameters dominate the different machining responses. It is possible that different operating points will differ in performance between the different metrics, where one may be increased while another is diminished.

Acknowledgements

This research is funded by the U.S. Army - Armament Research, Development and Engineering Center (ARDEC), Internal Lab Independent Research (ILIR) Grant; and the U.S Army-ARDEC, Science Fellowship Grant.

References

[1] F. Pitschke, General applications of electrochemical machining, Tech. rep., *SAE Technical Paper* (1962).

[2] M. Datta, D. Landolt, Electrochemical machining under pulsed current conditions, *Electrochimica Acta* **26** (7) (1981) 899-907.

[3] T. Masuzawa, M. Kimura, Electrochemical surface finishing of tungsten carbide alloy, *CIRP Annals-Manufacturing Technology* **40** (1) (1991) 199-202.

[4] A. Zaytsev, I. Agafonov, N. Gimaev, R. Moukhoutdinov, A. Belogorsky, Precise pulse electrochemical machining by bipolar current: Aspects of effective technological application, *Journal of materials processing technology* **149** (1) (2004) 419-425.

[5] R. Mathew, M. M. Sundaram, Modeling and fabrication of micro tools by pulsed electrochemical machining, *Journal of Materials Processing Technology* **212** (7) (2012) 1567-1572.

[6] W. Natsu, D. Kurahata, Observation of workpiece surface in ecm process of wc alloy micropin with bipolar pulses, *International Journal of Electrical Machining* **21** (2016) 31-38.

[7] P. B. Tailor, A. Agrawal, S. S. Joshi, Evolution of electrochemical finishing processes through cross innovations and modeling, *International Journal of Machine Tools and Manufacture* **66** (0) (2013)

[8] M. Inman, T. Hall, E. Taylor, C. Reece, O. Trofimova, Niobium electropolishing in an aqueous, non-viscous hf-free electrolyte: A new polishing mechanism, *SRF2011*, Chicago, IL June. (2011)

[9] J. W. Park, D. W. Lee, Pulse electrochemical polishing for microrecesses based on a coulostatic analysis, *The International Journal of Advanced Manufacturing Technology* **40** (7-8) (2009) 742-748.

[10] J. Fang, Z. Jin, W. Xu, Y. Shi, Magnetic electrochemical finishing machining, *Journal of materials processing technology* **129** (1) (2002) 283-287.

[11] O. Lioubashevski, E. Katz, I. Willner, Magnetic field effects on electrochemical processes: a theoretical hydrodynamic model, *The Journal of Physical Chemistry B* **108** (18) (2004) 5778-5784.

[12] Z. Fan, T. Wang, L. Zhong, The mechanism of improving machining accuracy of ecm by magnetic field, *Journal of materials processing technology* **149** (1) (2004) 409-413.

[13] L. Tang, W. Gan, Experiment and simulation Study on concentrated magnetic field-assisted ecm s-03 special stainless steel complex cavity, *The International Journal of Advanced Manufacturing Technology* **72** (5-8) (2014) 685-692.

[14] P. Pa, Design of a magnetic-assistance super finish module for freeform machining, *Journal of Vacuum Science & Technology B* **27** (3) (2009) 1221-1225.

[15] P. Pa, Mechanism design of magnetic-assistance in surface finishing of end-turning, *Journal of Advanced Mechanical Design, Systems, and Manufacturing* **2** (4) (2008) 587-596.

[16] L. Yin, W.M. Zhang, Y. Yan, Q.S. Tu, Z.J. Zhang, Study of electrochemical finishing with magnetic field and high-frequency group pulse, *Digital Manufacturing and Automation (ICDMA),*

2010 International Conference, Vol. **2**, IEEE, 2010, pp. 440-443.

[17] L. Long, M. Baoji, W. Ruifeng, D. Lingqi, The coupled effect of magnetic field, electric field, and electrolyte motion on the material removal amount in electrochemical machining, *The International Journal of Advanced Manufacturing Technology* (2017) 1-12.

[18] O. Weber, A. Rebschläger, P. Steuer, D. Bähre, Modeling of the material/electrolyte interface and the electrical current generated during the pulse electrochemical machining of grey cast iron, *Proceedings of the European COMSOL conference*. (2013)

[19] D. J. Griffiths, Electrodynamics, *Introduction to Electrodynamics, 3rd ed.*, Prentice Hall, Upper Saddle River, New Jersey (1999) 301-306

[20] Y. Marcus, Ions in water and biophysical implications: from chaos to cosmos, *Springer Science & Business Media*, (2012)

[21] R. S. Shevell, *Fundamentals of flight*, Pearson, (1989).

[22] A. Tavassoli, Assessment of austenitic stainless steels, *Fusion Engineering and Design* **29** (1995) 371-390.

[23] R. Stoltz, R. Pelloux, Inhibition of corrosion fatigue in 7075 aluminum alloys, *Corrosion* **29** (1) (1973) 13-17.

[24] G. Inzelt, A. Lewenstam, F. Scholz, *Handbook of reference electrodes*, Springer, (2013).

[25] W. Liu, S. Ao, Y. Li, Z. Liu, H. Zhang, S. M. Manladan, Z. Luo, Z. Wang, Effect of anodic behavior on electrochemical machining of tb6 titanium alloy, *Electrochimica Acta* **233** (2017) 190-200.

[26] M. Datta, D. Landolt, High rate transpassive dissolution of nickel with pulsating current, *Electrochimica Acta* **27** (3) (1982) 385-390.

[27] O. Weber, H. Natter, D. Bähre, Pulse electrochemical machining of cast iron: a layer-based approach for modeling the steady-state dissolution current, *Journal of Solid State Electrochemistry* **19** (5) (2015) 1265-1276.